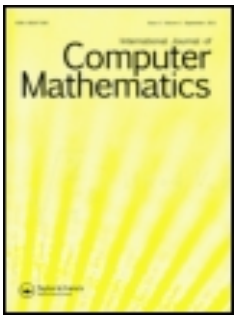

International Journal of Computer Mathematics

ISSN: 0020-7160 (Print) 1029-0265 (Online) Journal homepage: http://www.tandfonline.com/loi/gcom20

Finite volume approximation of stiff problems on two-dimensional curvilinear domain

Sylvain Faure, Mohamed Mahdi Tekitek & Roger Temam

To cite this article: Sylvain Faure, Mohamed Mahdi Tekitek & Roger Temam (2015): Finite volume approximation of stiff problems on two-dimensional curvilinear domain, International Journal of Computer Mathematics, DOI: 10.1080/00207160.2015.1075013

To link to this article: http://dx.doi.org/10.1080/00207160.2015.1075013

Accepted online: 27 Jul 2015.Published online: 11 Sep 2015.

International Journal of Computer Mathematics, 2015
http://dx.doi.org/10.1080/00207160.2015.1075013

Finite volume approximation of stiff problems on two-dimensional curvilinear domain

Sylvain Faure[a], Mohamed Mahdi Tekitek[b*] and Roger Temam[c]

[a]*Laboratoire de Mathématiques d'Orsay, Université Paris-Sud, 91405 Orsay, France;* [b]*Faculty of Sciences of Tunis, University of Tunis El Manar, El Manar, 2092 Tunis, Tunisia;* [c]*Institute for Scientific Computing and Applied Mathematics, Indiana University, Bloomington, IN 47405, USA*

(*Received 3 February 2015; revised version received 29 May 2015; accepted 16 June 2015*)

The aim of this article is to apply a novel finite volume method to approximate a stiff problem for a two-dimensional curvilinear domain. The stiffness is caused by the existence of a small parameter in the equation which introduces a boundary layer along parts of the curvilinear boundary. Incorporating in the finite volume space the boundary layer correctors, the boundary layer singularities are absorbed. Hence, we propose a second order scheme for curvilinear domains using uniform meshes thus avoiding the costly refinement of mesh in the boundary layers.

Keywords: finite volume methods; boundary layers; correctors; stiff problems

2010 AMS Subject Classifications: 65N08; 76F40; 65L04

1. Introduction

We consider the following reaction-diffusion problem in a two-dimensional domain:

$$\begin{aligned} -\varepsilon\Delta u + bu &= f, \quad \text{in } \Omega, \\ u(x,y) &= u_1(x,y), \quad \text{on } \Gamma_1, \\ u(x,y) &= u_2(x,y), \quad \text{on } \Gamma_2, \end{aligned} \tag{1}$$

where $\Omega = \{(x,y) \in \mathbb{R}^2, R_1 < x^2 + y^2 < R_2\}$, f, u_1 and u_2 are sufficiently smooth, $b \geq \delta > 0$, $R_1 < R_2$ and $\varepsilon > 0$. We assume the Dirichlet boundary condition on $\Gamma_1 = \{(x,y) \in \mathbb{R}^2, x^2 + y^2 = R_1\}$, and $\Gamma_2 = \{(x,y) \in \mathbb{R}^2, x^2 + y^2 = R_2\}$. For ε small, the solution u^ε of problem (1) possesses boundary layers at the boundaries Γ_1 and Γ_2. The analysis of such singularly perturbed problems can be found for example in [7,8,12–14,24,26], and for the numerical approach see for example [10,15,16].

Our purpose here is to adapt the method applied in [19] to problem (1). In fact we show how to implement an enriched subspace technique in the context of finite volumes (see e.g. [9]).

The concept of enriched subspace technique has recently developed in many different directions. It consists in adding to the Galerkin or similar basis, one or more functions which carry

*Corresponding author. Email: mahdi.tekitek@math.u-psud.fr

the singularity of the problem. In [14], it consists in adding to the Galerkin basis functions correctors which correspond to the boundary layer singularity in the case of singular perturbation problems; see more recently [2,3,16–19] and the references therein. The concept of enriched spaces has been also introduced in the approximation of cracks and other singular problems under the names of XFEM (extended Finite Element Method) and GFEM (generalized FEM); see for example [1,21–23]. The other specific aspect of this work is that the space discretization is made by a finite volume method, whereas finite elements are much more common in this context; and finally the domain is curved. Indeed, the major difference and difficulty here is the domain which has a curvilinear boundary whereas Ω is a rectangle in [19]. In our case, as always, the boundary layer correctors are one-dimensional functions in the direction orthogonal to the boundary; (see e.g. [11,12]). Hence we can obtain explicit forms of the correctors and incorporate them in the finite volume space. Thus the advantage of this method is that we avoid mesh refinement and still produce a second order accuracy method using uniform meshes. In Section 2, we will recall a finite volume scheme usually used in curvilinear mesh. Then the correctors will be added in Section 3 and the numerical results are given in Section 4.

2. Classical finite volume schemes

We consider a finite volume discretization of the space $H_0^1(\Omega)$; as indicated above Ω is an annulus for simplicity, but more general domains of similar topology can be considered. Let $\mathcal{T}$ be a structured mesh such that $\mathcal{T} = (K_{i,j})_{i=1,\dots,M,\ j=1,\dots,N}$ where an element of $\mathcal{T}$, denoted by $K_{i,j}$ is quadrangular and is called a control volume (cell). As shown in Figure 1, each $K_{i,j}$ is the quadrangle represented in polar coordinates by its vertices $(R_1 + m\Delta r, n\Delta\theta), m = i, i+1, n = j, j+1$ with $M\Delta r = R_2 - R_1$ and $N\Delta\theta = 2\pi$, $m = 0, \dots, M$, $n = 0, \dots N$. The vertices of the cells are thus points with polar coordinates $r_i = i\Delta r$ and $\theta_j = j\Delta\theta$. We denote by $x_{i,j}$ the center of gravity of the cell $K_{i,j}$ and $x_{i,j+1/2}$, $x_{i,j-1/2}$, $x_{i+1/2,j}$, and $x_{i-1/2,j}$ are the center of the edges of the control volume $K_{i,j}$ (see Figure 2). We introduce the characterestic function $\chi_{i,j}$ equal to 1 over the control volume $K_{i,j}$ and 0 elsewhere.

Multiplying (1) by the characterestic function $\chi_{i,j}$, integrating over Ω and applying the divergence theorem we find :

$$-\varepsilon \int_{\partial K_{i,j}} \frac{\partial u}{\partial \nu} + \int_{K_{i,j}} bu = \int_{K_{i,j}} f, \tag{2}$$

where ν is the unit outward normal at the boundary of $\partial K_{i,j}$. Let us denote by $u_{i,j}$, the discrete unknown associated with the control volume $K_{i,j} \in \mathcal{T}$. So to build our scheme we classically have to approximate the quantity $\partial u/\partial \nu$ on the different edges of $\partial K_{i,j}$ by using these discrete unknowns. To this purpose we use a 9-points scheme [9]. Let us consider the configuration described in Figure 3, which is a generic configuration of structured mesh $\mathcal{T}$; K is the cell of interest, L and M are its direct neighbors, ν_{KL} is the normal to the common edge $[KL]$ of K and L. The flux $\nabla u \cdot \nu_{KL}$ on the edge between the cells L and K is approximated by:

$$\nabla u \cdot \nu_{KL} = \frac{u_E - u_W}{d(E,W)},$$

where $d(E,W)$ is the distance between the points E and W, u_E and u_W are the approximate values of u, respectively, at the points E and W where the orthogonal bisector of the edge $[KL]$ intersects the segment $[C_K, C_M]$ and E is defined similarly.

Now we have to approximate u_W with the values of u in the center of gravity of L and N. In fact, for the geometry described in Figure 3, the following linear interpolation formula can be

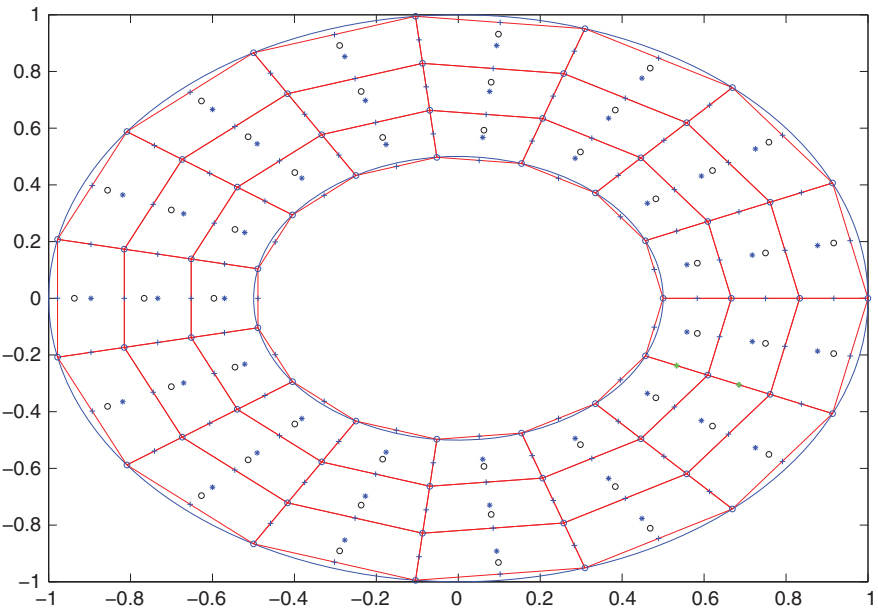

Figure 1. Structured mesh of Ω, $x_{ij} = *$ denotes the center of gravity of the cells and $+$ denotes the center of the edges. In this case $M = 3$ and $N = 15$, i.e. $i = 1, 2, 3$ and $j = 1, 2, \ldots, 15$.

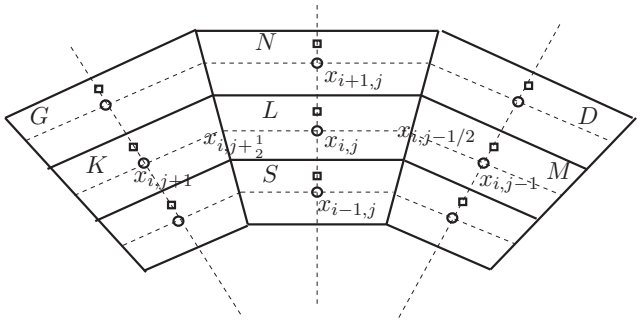

Figure 2. Cells around $K_{i,j}$, where $x_{ij} = \mathrm{o}$ denotes the center of gravity of the cell, $\square$ intersection of the orthogonal bisector of the edges $\theta = \theta_i$ and suitable segments connecting the centers $x_{m,n}$.

used:

$$u_W \simeq \frac{\alpha u_K + \beta u_M}{\alpha + \beta};$$

here $\alpha = d(W, C_M)$ and $\beta = d(W, C_K)$. Note that the adjacent cell M is chosen so that W is in the interior of the segment $[C_K, C_M]$; For the value u_E we do the same approximation using the values of u in the centers of gravity of L and N, where the cell N is introduced in the context of Figure 3.

The description above relates to the particular mesh given by Figure 2, which is a zoom of the structured mesh $\mathcal{T}$ described by Figure 1. Applying the 9-points finite volumes scheme in this geometry we obtain the following formula for the flux of $\partial u/\partial \nu$ on the edges ∂K_L of the cell K_L

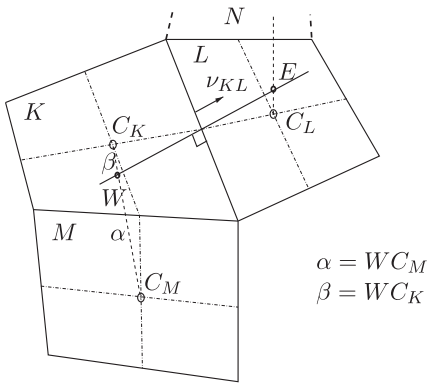

Figure 3. Cells around K, also written L where $\alpha = d(W, C_M)$ denotes the distance between W and C_M and $\beta = d(W, C_K)$ denotes the distance between W and C_K.

which denotes volume L in Figure 2:

$$\int_{\partial K_L} \frac{\partial u}{\partial \nu} \simeq |LN| \frac{u_N - u_L}{d_N} + |LS| \frac{u_S - u_L}{d_S} + \frac{|LE|}{d^*} \left[\frac{\alpha u_D + \beta u_M}{\alpha + \beta} - \frac{\alpha u_N + \beta u_L}{\alpha + \beta} \right] + \frac{|LW|}{d^*} \left[\frac{\alpha u_G + \beta u_K}{\alpha + \beta} - \frac{\alpha u_N + \beta u_L}{\alpha + \beta} \right]. \tag{3}$$

Here $|LN|$ is the length of the common edge of the volumes L and N. The quantities d_N, d_S are respectively, the distance between the cell's center of L and N (i.e. $d_N = d(x_{i,j}, x_{i+1,j})$) and the distance between the cell's center of L and S (i.e. $d_S = d(x_{i,j}, x_{i-1,j})$) and d^* is the distance between the centers of gravity of the two cells L and M or L and K (i.e. $d^* = d(x_{i,j}, x_{i,j+1}) = d(x_{i,j}, x_{i,j-1})$). The numerical gradient ∇u in the cell $K_{i,j}$ is given in polar coordinates by:

$$\nabla^\theta u \simeq \frac{1}{d^*} \left[\frac{\alpha u_D + \beta u_M}{\alpha + \beta} - \frac{\alpha u_N + \beta u_L}{\alpha + \beta} \right], \tag{4}$$

$$\nabla^r u \simeq \frac{u_N - u_L}{d_N}. \tag{5}$$

So we obtain the 9-point finite volumes scheme corresponding to Equation (2) for the cell $L = K_{i,j}$:

$$-\varepsilon \left(|LN| \frac{u_{i+1,j} - u_{i,j}}{d_N} + |LS| \frac{u_{i-1,j} - u_{i,j}}{d_S} + \frac{|LE|}{d^*} \left[\frac{\alpha u_{i+1,j-1} + \beta u_{i,j-1}}{\alpha + \beta} - \frac{\alpha u_{i+1,j} + \beta u_{i,j}}{\alpha + \beta} \right] + \frac{|LW|}{d^*} \left[\frac{\alpha u_{i+1,j+1} + \beta u_{i,j+1}}{\alpha + \beta} - \frac{\alpha u_{i+1,j} + \beta u_{i,j}}{\alpha + \beta} \right] \right) + b|K_{i,j}|u_{i,j} = |K_{i,j}|f_{i,j}, \tag{6}$$

where $i = 2, \ldots, M-1$ and $j = 1, \ldots, N$. To impose the Dirichlet boundary condition on $\partial\Omega$, we add the known values (equal to the Dirichlet condition given by the second and third equations of problem (1)) on the center of the edges which are in $\partial\Omega$. Therefore for the cell which has an edge which belongs to the boundary (i.e. $i = 1$ or $i = M$) we obtain the same formula as (6) where d_N is replaced by $d_N/2$ if the cell is on the external boundary and d_S is replaced by $d_S/2$ if the cell is on the internal boundary.

Remark We note, here, that to impose the Dirichlet boundary conditions, we do not add fictitious nodes but we rather consider that we have a cell control with zero area on the boundary edges.

3. Finite volume schemes with correctors

Without loss of generality, we consider the following problem :

$$\begin{aligned} -\varepsilon\Delta u + u &= f, \quad \text{in } \Omega, \\ u(x,y) &= \frac{1}{2}, \quad \text{on } \Gamma_1, \\ u(x,y) &= 0, \quad \text{on } \Gamma_2, \end{aligned} \tag{7}$$

where f $= 1/2$ on Γ_1. In this case we expect boundary layers at the external boundary Γ_2 only. In fact the exact solution u can be decomposed as $u = u^f + u^s$, where u^s represents the smooth part of u and u^f is its fast part (see [18]). We consider new schemes incorporating the correctors which absorb the stiffness of the solution. So the stiff part u^f will be the corrector function given in polar coordinates by:

$$\varphi(r) = -\exp\left(\frac{r - R_2}{\sqrt{\varepsilon}}\right). \tag{8}$$

On the other hand, we use classical finite volume methods (cFVM) described in the previous section to approximate the non-stiff part u^s. Thus we approximate the solution $u = u^s + u^f$, in the enriched space, by the discrete solution u_h given by:

$$u_h = \sum_{j=1}^{N} \xi_j \varphi \chi_{M,j} + \sum_{i,j} u_{i,j}\chi_{i,j}, \quad \text{for } i = 1,\ldots,M,\ j = 1,\ldots,N.$$

A crucial point here, is that we have N more unknowns, that is, the ξ_j corresponding to the added elements. They will be determined using the correctors $\varphi\chi_{M,j}$ as test elements. So we start with the generic test elements $\chi_{i,j}$. For $1 \le i \le M,\ 1 \le j \le N$, multiplying the first equation of (7) by $\chi_{i,j}$ and integrating over $K_{i,j}$ we find the equations that are equivalent to those of the classical 9-point FV scheme. Multiplying then the first equation of (7) by $\varphi\chi_{M,j}$, $j = 1,\ldots,N$, and integrating over Ω we find:

$$-\varepsilon\int_{\partial K_{M,j}} \varphi\frac{\partial u}{\partial \nu} + \varepsilon\int_{K_{M,j}} \nabla u\nabla\varphi + \int_{K_{M,j}} u\varphi = \int_{K_{M,j}} f\varphi. \tag{9}$$

Using the numerical approximation of ∇u given by Equations (4) and (5) we compute the different terms of Equation (9). In fact the first term gives the following expression:

$$\begin{aligned} \int_{\partial K_{M,j}} \varphi\frac{\partial u}{\partial \nu} \simeq{}& \frac{\xi_j - u_L}{\tilde{d}_N}\int_{\partial N}\varphi + \frac{u_S - u_L}{d_S}\int_{\partial S}\varphi + \frac{1}{d^*}\left[\frac{\alpha\xi_{j-1} + \beta u_M}{\alpha+\beta} - \frac{\alpha\xi_j + \beta u_L}{\alpha+\beta}\right]\int_{\partial E}\varphi \\ &+ \frac{1}{d^*}\left[\frac{\alpha\xi_{j+1} + \beta u_K}{\alpha+\beta} - \frac{\alpha\xi_j + \beta u_L}{\alpha+\beta}\right]\int_{\partial W}\varphi. \end{aligned}$$

where $\tilde{d}_N = d_N/2$ because the edge ∂N of the cell $K_{M,j}$ belongs to Γ_2. Now we will compute every term of the above equation by replacing φ by its expression in Equation (8). So the

boundary integrals $\int \theta$ give:

$$\int_{\partial N} \varphi = -|LN|,$$
$$\int_{\partial S} \varphi = -|LS| \mathrm{e}^{(\bar{r}-R_2)/\sqrt{\varepsilon}},$$
$$\int_{\partial E} \varphi = \int_{\bar{r}}^{R_2} -\mathrm{e}^{(r-R_2)/\sqrt{\varepsilon}} = (\mathrm{e}^{(\bar{r}-R_2)/\sqrt{\varepsilon}} - 1)\sqrt{\varepsilon} = C,$$
$$\int_{\partial W} \varphi = \int_{\bar{r}}^{R_2} -\mathrm{e}^{(r-R_2)/\sqrt{\varepsilon}} = (\mathrm{e}^{(\bar{r}-R_2)/\sqrt{\varepsilon}} - 1)\sqrt{\varepsilon} = C.$$

The second term of Equation (9) gives:

$$\int_{K_{M,j}} \nabla u \nabla \varphi = \int_{\bar{r}}^{R_2} \int_{\theta_1}^{\theta_2} \frac{\partial \varphi}{\partial r} \frac{\partial u}{\partial r} r \, \mathrm{d}r \, \mathrm{d}\theta$$
$$= \frac{u_L - u_S}{d_S} \int_{\theta_1}^{\theta_2} \int_{\bar{r}}^{r^*} \frac{\partial \varphi}{\partial r} r \, \mathrm{d}r \, \mathrm{d}\theta + \frac{\xi_j - u_L}{\tilde{d}_N} \int_{\theta_1}^{\theta_2} \int_{r^*}^{R_2} \frac{\partial \varphi}{\partial r} r \, \mathrm{d}r \, \mathrm{d}\theta.$$

Here θ_1, θ_2, and $\bar{r}$ are the polar coordinates of the vertices of the cell $K_{M,j}$ and the scalar r^* is given by $r^* = (R_2 + \bar{r})/2$. Replacing now φ by its expression in Equation (8), in the above equation, we find that we have to calculate the following quantity:

$$\int_{r_1}^{r_2} r \, \mathrm{e}^{(r-1)/\sqrt{\varepsilon}} \mathrm{d}r = [\sqrt{\varepsilon}(r - \sqrt{\varepsilon}) \, \mathrm{e}^{(r-1)/\sqrt{\varepsilon}}]_{r_1}^{r_2},$$

where $r_1 = \bar{r}$, $r_2 = r^*$ in the first case and $r_1 = r^*$, $r_2 = R_2$ in the second case. So let

$$A = \int_{\bar{r}}^{r^*} \frac{\partial \varphi}{\partial r} r \, \mathrm{d}r = [(\sqrt{\varepsilon} - r) \, \mathrm{e}^{(r-R_2)/\sqrt{\varepsilon}}]_{\bar{r}}^{r^*} = (\sqrt{\varepsilon} - r^*) \, \mathrm{e}^{(r^*-R_2)/\sqrt{\varepsilon}} - (\sqrt{\varepsilon} - \bar{r}) \, \mathrm{e}^{(\bar{r}-R_2)/\sqrt{\varepsilon}},$$

and

$$B = \int_{r^*}^{R_2} \frac{\partial \varphi}{\partial r} r \, \mathrm{d}r = [(\sqrt{\varepsilon} - r) \, \mathrm{e}^{(r-R_2)/\sqrt{\varepsilon}}]_{r^*}^{R_2} = (\sqrt{\varepsilon} - R_2) - (\sqrt{\varepsilon} - r^*) \, \mathrm{e}^{(r^*-R_2)/\sqrt{\varepsilon}}.$$

We conclude that the second term of Equation (9) is given by:

$$\int_{K_j} \nabla u \nabla \varphi = \frac{u_L - u_S}{d_S} A(\theta_2 - \theta_1) + \frac{\xi_j - u_L}{\tilde{d}_N} B(\theta_2 - \theta_1).$$

We compute now the third term of Equation (9):

$$\int_{K_j} u\varphi = u_L \int_{K_j} \varphi$$
$$= u_L[\sqrt{\varepsilon}(\sqrt{\varepsilon} - R_2) + \sqrt{\varepsilon}(\bar{r} - R_2) \, \mathrm{e}^{(\bar{r}-R_2)/\sqrt{\varepsilon}}](\theta_2 - \theta_1)$$
$$= u_L D(\theta_2 - \theta_1),$$

where $D = [\sqrt{\varepsilon}(\sqrt{\varepsilon} - R_2) + \sqrt{\varepsilon}(\bar{r} - R_2) \, \mathrm{e}^{(\bar{r}-R_2)/\sqrt{\varepsilon}}]$.

Using these results, Equation (9) becomes:

$$-\varepsilon\left[\frac{\xi_j-u_L}{\tilde{d}_N}(-|LN|)+\frac{u_S-u_L}{d_S}(-|LS|\mathrm{e}^{(\bar{r}-R_2)/\sqrt{\varepsilon}})+\frac{C}{d^*}\left(\frac{\alpha\xi_{j-1}+\beta u_M}{\alpha+\beta}-\frac{\alpha\xi_j+\beta u_L}{\alpha+\beta}\right)\right.$$
$$\left.+\frac{C}{d^*}\left(\frac{\alpha\xi_{j+1}+\beta u_K}{\alpha+\beta}-\frac{\alpha\xi_j+\beta u_L}{\alpha+\beta}\right)\right]+\varepsilon\left[\frac{u_L-u_S}{d_S}A(\theta_2-\theta_1)+\frac{\xi_j-u_L}{\tilde{d}_N}B(\theta_2-\theta_1)\right]$$
$$+D\,u_L(\theta_2-\theta_1)=\int_{K_j}f\varphi.$$

We rewrite the above equation as follows:

$$-\varepsilon\left[\frac{C}{d^*}\frac{\alpha}{\alpha+\beta}\xi_{j-1}+\frac{C}{d^*}\frac{\alpha}{\alpha+\beta}\xi_{j+1}+\frac{C}{d^*}\frac{\beta}{\alpha+\beta}u_M+\frac{C}{d^*}\frac{\beta}{\alpha+\beta}u_K\right]$$
$$+\varepsilon\left[\frac{|LS|}{d_S}\mathrm{e}^{(\bar{r}-R_2)/\sqrt{\varepsilon}}-\frac{A}{d_S}(\theta_2-\theta_1)\right]u_S+\varepsilon\left[\frac{|LN|}{\tilde{d}_N}+2\frac{C}{d^*}\frac{\alpha}{\alpha+\beta}+\frac{B}{\tilde{d}_N}(\theta_2-\theta_1)\right]\xi_j$$
$$+\varepsilon\left[-\frac{|LN|}{\tilde{d}_N}-\frac{|LS|}{d_S}\mathrm{e}^{(\bar{r}-R_2)/\sqrt{\varepsilon}}+2\frac{C}{d^*}\frac{\beta}{\alpha+\beta}+\frac{A}{d_S}(\theta_2-\theta_1)-\frac{B}{\tilde{d}_N}(\theta_2-\theta_1)\right]u_L$$
$$+D(\theta_2-\theta_1)u_L=D(\theta_2-\theta_1)f_j.$$

Finally using the numbering of the nodes we can rewrite the above equations in the following form:

$$-\varepsilon\left[\frac{C}{d^*}\frac{\alpha}{\alpha+\beta}\xi_{j-1}+\frac{C}{d^*}\frac{\alpha}{\alpha+\beta}\xi_{j+1}+\frac{C}{d^*}\frac{\beta}{\alpha+\beta}u_{M,j-1}+\frac{C}{d^*}\frac{\beta}{\alpha+\beta}u_{M,j+1}\right]$$
$$+\varepsilon\left[\frac{|LS|}{d_S}\mathrm{e}^{(\bar{r}-R_2)/\sqrt{\varepsilon}}-\frac{A}{d_S}(\theta_2-\theta_1)\right]u_{M-1,j}+\varepsilon\left[\frac{|LN|}{\tilde{d}_N}+2\frac{C}{d^*}\frac{\alpha}{\alpha+\beta}+\frac{B}{\tilde{d}_N}(\theta_2-\theta_1)\right]\xi_j$$
$$+\varepsilon\left[-\frac{|LN|}{\tilde{d}_N}-\frac{|LS|}{d_S}\mathrm{e}^{(\bar{r}-R_2)/\sqrt{\varepsilon}}+2\frac{C}{d^*}\frac{\beta}{\alpha+\beta}+\frac{A}{d_S}(\theta_2-\theta_1)-\frac{B}{\tilde{d}_N}(\theta_2-\theta_1)\right]u_{M,j}$$
$$+D(\theta_2-\theta_1)u_{M,j}=D(\theta_2-\theta_1)f_j,$$

where $i=M$ and $j=1,\ldots,N$. These equations are the new equations specific to the use of the correctors at the boundary. They are coupled with the classical finite volumes equations, that is, the Equations (6) with just the addition of those corresponding to the corrector φ.

4. Numerical results

We consider here the problem (7) with $R_1=\frac{1}{2}$, $R_2=1$, $f(x,y)=\sqrt{x^2+y^2}$, $u(x,y)=\frac{1}{2}$ on Γ_1 (Dirichlet condition at the interior boundary of the domain) and $u(x,y)=0$ on Γ_2 (Dirichlet condition at the exterior boundary of the domain). To validate our scheme, as we do not have the exact solution of the problem (7), we use the classical cFVM with an extremely fine mesh. This provides us a reference numerical solution called u_{ref}. Figure 4 shows the reference solution u_{ref} of problem (7) using classical finite volumes methods (cFVM), for mesh size $M=3$, $N=281$ and $\varepsilon=10^{-3}$.

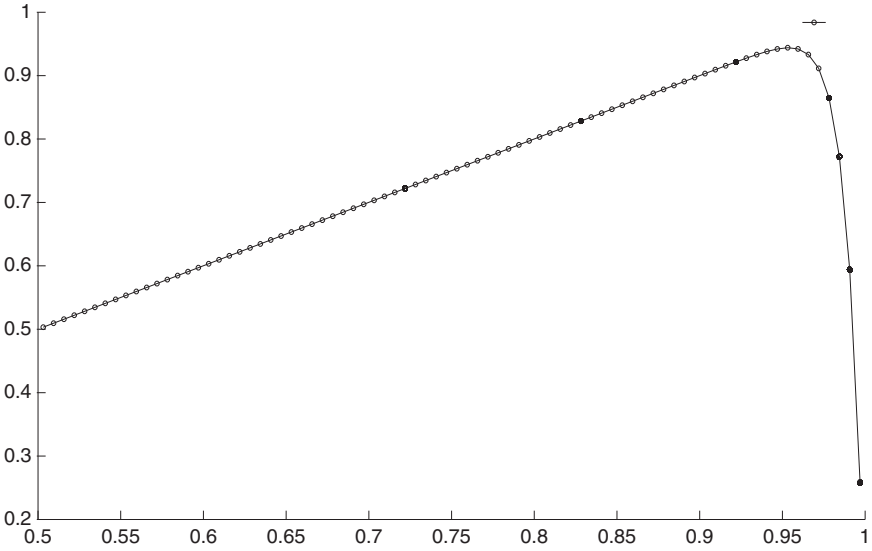

Figure 4. The reference solution *vs* $x_{1,j}, j = 1, \ldots, N$ where $\varepsilon = 10^{-3}$ and mesh size given by $= 3 \times 281$ using cFVM.

Table 1. The numerical accuracies, measured by the ℓ^∞ norm $\max_{1 \le j \le N}\{|u_{\text{ref}}(x_j) - u_j|\}$, where $u_{\text{ref}}(x_j)$ is the reference solution of problem (7) where $\varepsilon = 10^{-3}$.

$M \times N$	cFVM	nFVM
3×11	0.136	2.85×10^{-3}
3×21	6.52×10^{-2}	8.53×10^{-4}
3×41	2.21×10^{-2}	5.06×10^{-4}
3×81	6.11×10^{-3}	4.39×10^{-5}

Table 1 shows the ℓ^∞ error given by $\sup_j\{|u_{\text{ref}}(x_j) - u_j|\}$ where $u_{\text{ref}}(x_j)$ is the reference solution and u_j is the solution of problem (7), without and with correctors (i.e. using cFVM and nFVM). As it appears in this table, the new finite volume methods (nFVM) attains a much better numerical accuracy than the cFVM for $\varepsilon = 10^{-3}$.

Figure 5 shows the difference between the reference solution obtained using the correctors (nFVM) and that obtained without the correctors (i.e. cFVM). We clearly observe that the difference is concentrated on the boundary Γ_2 (i.e. $r = 1$) where the boundary layers singularities appears. This confirms that the better accuracy of the nFVM is due to the treatment of the boundary layer.

Figures 5 and 6, respectively, show the difference between the reference solution of problem 7 and the solution obtained with and without using correctors. We remark that the essential part of the error made by the cFVM method is located at the external boundary of the domain $r = 1$, that is at the boundary layer.

To achieve the validation of the new finite volumes scheme with correctors, we compute and compare the order of accuracy of the nFVM and cFVM methods, for different values of ε. Figures 7–9 show the curves of the ℓ^∞ errors between the numerical solution u obtained with and without using correctors and the reference solution u_{ref}, where $\varepsilon = 10^{-2}, 10^{-3}$ and 10^{-4}. Figures 7–9 show experimentally that the two methods have a second order accuracy.

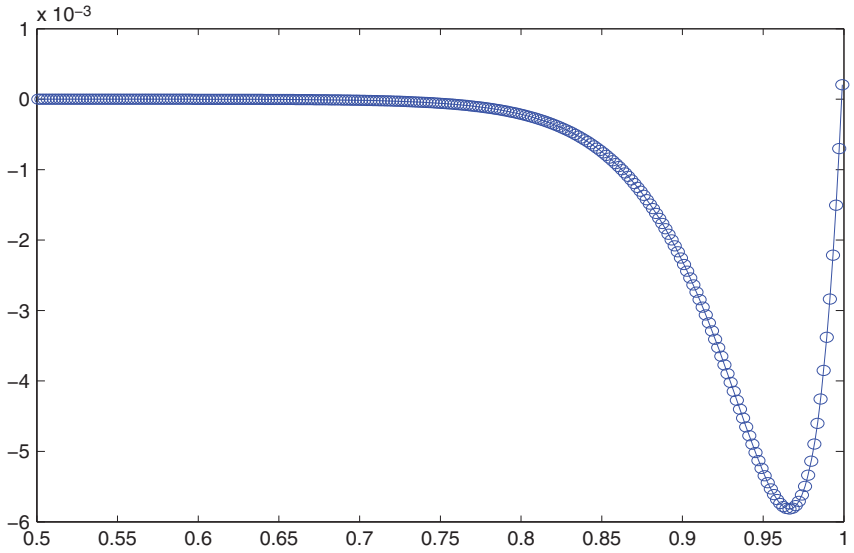

Figure 5. Difference between the solution u obtained by nFVM (i.e. using correctors) of problem (7) and the solution u obtained by cFVM (i.e. without correctors) of the same problem, where $\varepsilon = 10^{-3}$ and size of mesh is 3×281.

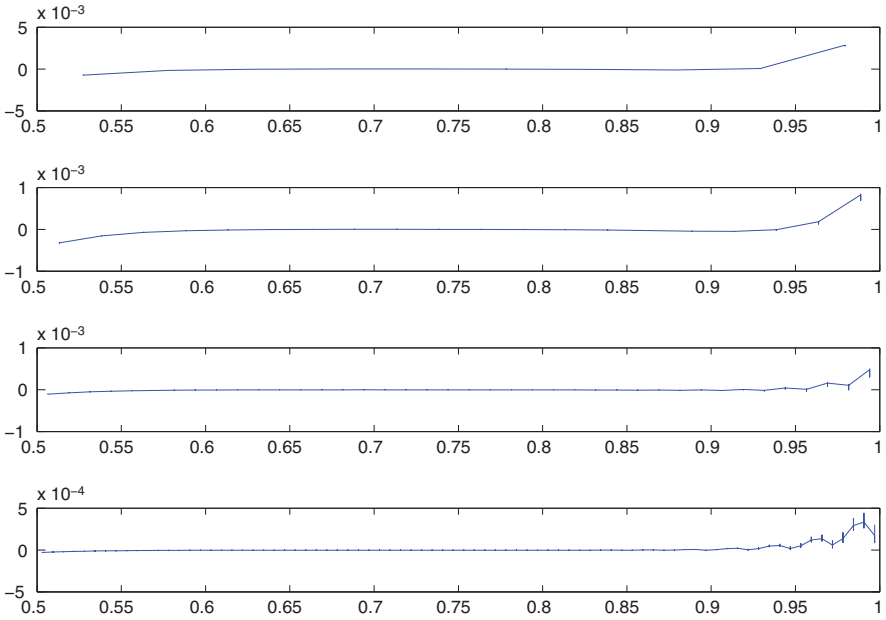

Figure 6. Error $\{|u_{\text{ref}}(x_j) - u_j|\}$, *vs* r, where u_j is the numerical solution of the problem (7) with corrector (nFVM) and $u_{\text{ref}}(x_j)$ is the reference solution where $\varepsilon = 10^{-3}$. The solution u_j is computed for different mesh size: from the top 3×11, 3×21, 3×41, and 3×81.

As shown in Figures 6 and 10, the numerical solution obtained using the nFVM method are stable and capture the boundary with economical mesh sizes. The cFVM method produces errors located in the boundary layer and we have to consider highly fine meshes to capture the stiffness.

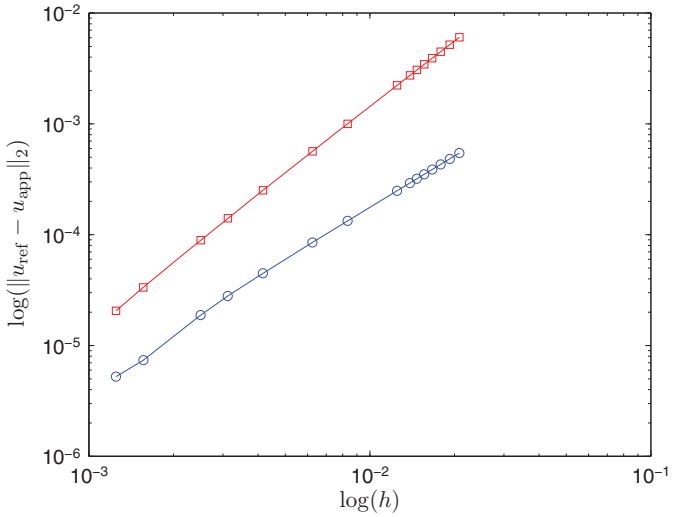

Figure 7. Convergence for $\varepsilon = 0.01$: ◯ The ℓ^2 error $u_{\text{ref}} - u_{\text{app}}$ *vs* $\log(h)$ where u_{app} is obtained using correctors (nFVM). □ The ℓ^2 error $u_{\text{ref}} - u_{\text{app}}$ *vs* $\log(h)$ where u_{app} is obtained without corrector (cFVM).

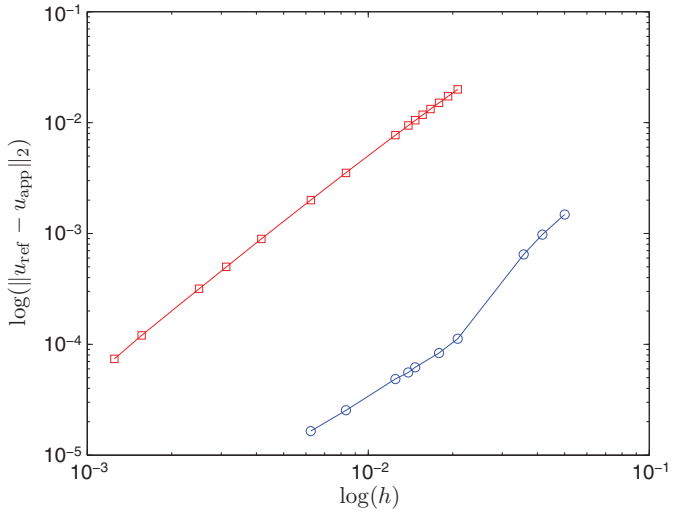

Figure 8. Convergence for $\varepsilon = 0.001$: ◯ The ℓ^2 error $u_{\text{ref}} - u_{\text{app}}$ *vs* $\log(h)$ where u_{app} is obtained using correctors (nFVM). □ The ℓ^2 error $u_{\text{ref}} - u_{\text{app}}$ *vs* $\log(h)$ where u_{app} is obtained without corrector (cFVM).

Figure 11 shows the cpu time to inverse the matrix of the discretization of the nFVM *vs* mesh size h. We observe that the cpu time is proportional to the mesh size h.

Finally we focus on the condition number of the discretization matrix of each method (i.e. cFVM and nFVM) in function of the mesh size h where $\varepsilon = 0.0001$. Figure 12 shows that for a more refined mesh (i.e. as the mesh size h decreases) the condition number of the two methods increases. On the other hand for a fixed mesh size h the condition number of the matrix using the correctors for (nFVM) is slightly larger than for (cFVM) and this is due to the size of the matrix since nFVM is larger than with cFVM.

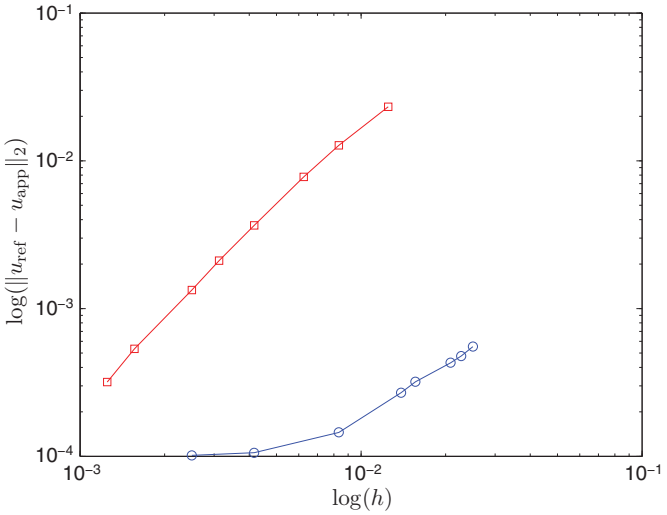

Figure 9. Convergence for $\varepsilon = 0.0001$: ◯ The ℓ^2 error $u_{\text{ref}} - u_{\text{app}}$ *vs* $\log(h)$ where u_{app} is obtained using correctors (nFVM). □ The ℓ^2 error $u_{\text{ref}} - u_{\text{app}}$ *vs* $\log(h)$ where u_{app} is obtained without corrector (cFVM).

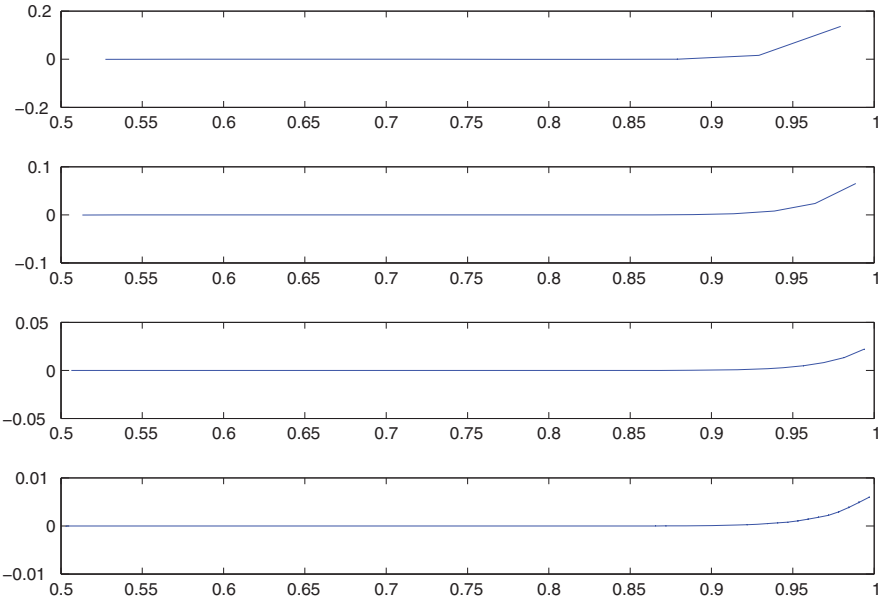

Figure 10. Error $\{|u_{\text{ref}}(x_j) - u_j|\}$, *vs* r, where u_j is the numerical solution of the problem (7) without corrector (cFVM) and $u_{\text{ref}}(x_j)$ is the reference solution where $\varepsilon = 10^{-3}$. The solution u_j is computed for different mesh size: from the top 3×11, 3×21, 3×41, and 3×81.

5. Conclusion

We have extended the 2D work of [19] to a curvilinear domain. We have shown that the corrector absorbs the boundary layer and that we are able to achieve a second order numerical accuracy. Thus we have avoided refining the mesh in the boundary layers as $\varepsilon \to 0$.

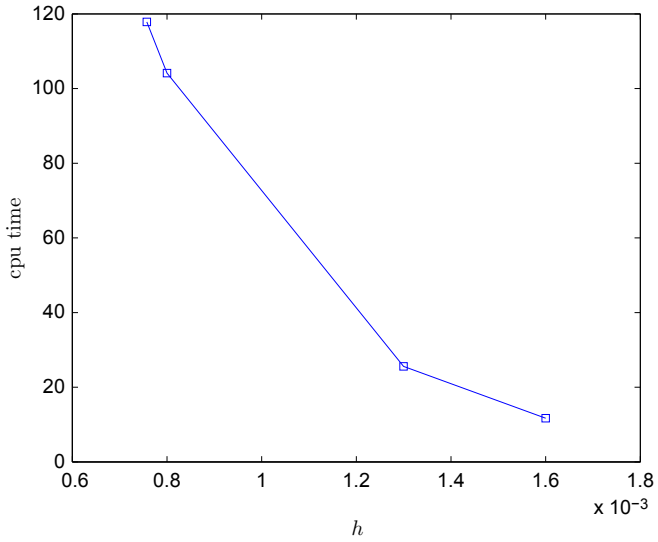

Figure 11. Time of inversion of the matrix *vs* mesh size h for $\varepsilon = 0.001$.

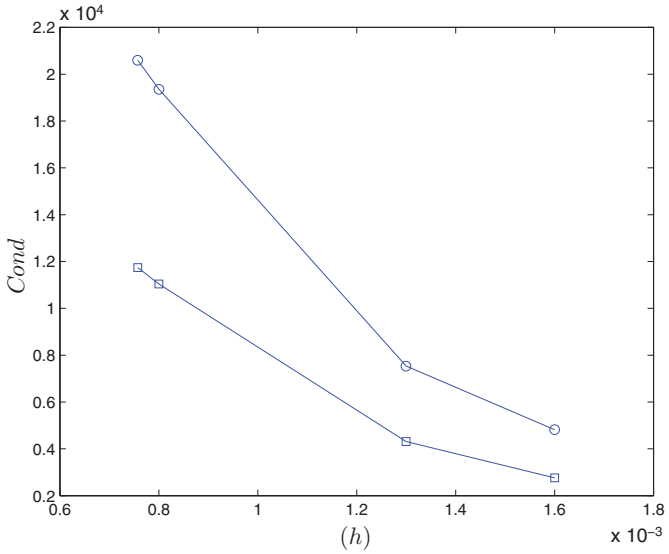

Figure 12. Condition number of the matrix *vs* mesh size h, where $\varepsilon = 0.0001$: ◯ with correctors (nFVM) where the size of the matrix is $(M+1)N \times (M+1)N$, □ without correctors (cFVM) where the size of the matrix is $MN \times MN$.

In future works we want to extend our method to more complex problems. Here we note that the boundary layer correctors are still one-dimensional. We may also consider more general elliptic operators of second or higher order, or time dependent problems (see [4–6,20]). Finally we will extend our method to resolve convection-diffusion equations [19,25,27].

Disclosure

No potential conflict of interest was reported by the authors.

Funding

This work was supported in part by the NSF Grants DMS 1206438, and by the Research Fund of Indiana University.

References

[1] I. Babuška and J.M. Melenk, *The partition of unity method*, Int. J. Numer. Meth. Eng. 40 (1997), pp. 727–758.
[2] W. Cheng and R. Temam, *Numerical approximation of one-dimensional stationary diffusion equations with boundary layers*, Comput. Fluids 31 (2002), pp. 453–466.
[3] W. Cheng, R. Temam and X. Wang, *New approximation algorithms for a class of partial differential equations displaying boundary layer behavior, Dedicated to Cathleen Morawetz on her 75th birthday*, Meth. Appl. Anal. 7 (2000), pp. 363–390.
[4] B. Cockburn and C.-W. Shu, *Runge-Kutta discontinuous Galerkin methods for convection-dominated problems*, J. Sci. Comput. 16 (2001), pp. 173–261.
[5] B. Cockburn, F. Coquel and P.G. LeFloch, *Convergence of the finite volume method for multidimensional conservation laws*, SIAM J. Numer. Anal. 32 (1995), pp. 687–705.
[6] B. Cockburn, G. Kanschat and D. Schotzau, *A locally conservative LDG method for the incompressible Navier-Stokes equations*, Math. Comput. 74 (2005), pp. 1067–1095.
[7] W. Eckhaus, *Boundary layers in linear elliptic singular perturbation problems*, SIAM Rev. 14 (1972), pp. 225–270.
[8] W. Eckhaus and E.M. De Jager, *Asymptotic solutions of singular perturbation problems for linear differential equations of elliptic type*, Arch. Rational Mech. Anal. 23 (1966), pp. 26–86.
[9] R. Eymard, T. Gallouet and R. Herbin, *Finite Volume Methods*, Handbook of Numerical Analysis, vol. VII, North-Holland, 2000, pp. 713–1020.
[10] S. Faure, D. Pham and R. Temam, *Comparison of finite volume and finite difference methods and application*, Anal. Appl. 4 (2006), pp. 163–208.
[11] G. Gie, *Singular perturbation problems in a general smooth domain*, Asymptot. Anal. 6 (2009), pp. 227–249.
[12] G. Gie, M. Hamouda and R. Temam, *Boundary layers in smooth curvilinear domains: parabolic problems*, Discrete Contin. Dyn. Syst. 26 (2010), pp. 1213–1240.
[13] M. Hamouda, C. Jung and R. Temam, *Boundary layers for the 2D linearized primitive equations*, Comm. Pure Appl. Anal. 8 (2009), pp. 335–359.
[14] H. Han and R.B. Kellogg, *A method of enriched subspaces for the numerical solution of a parabolic singular perturbation problem*, Comput. Asymp. Meth. Boun. Inter. Layer 4 (1982), pp. 46–52. Dublin.
[15] C.-Y. Jung, *Numerical approximation of two-dimensional convection-diffusion equations with boundary layers*, Numer. Meth. Part. Diff. Eq. 21 (2005), pp. 623–648.
[16] C. Jung and R. Temam, *Numerical approximation of two-dimensional convection-diffusion equations with multiple boundary layers*, Internat. J. Numer. Anal. Model. 2 (2005), pp. 367–408.
[17] C. Jung and R. Temam, *Asymptotic analysis for singularly perturbed convection-diffusion equations with a turning point*, J. Math. Phys. 48 (2007), p. 27.
[18] C.Y. Jung and R. Temam, *Finite volume approximation of one-dimensional stiff convection-diffusion equations*, J. Sci. Comput. 41 (2009), pp. 384–410.
[19] C. Jung and R. Temam, *Finite volume approximation of two-dimensional stiff problems*, INJAM 7 (2010), pp. 462–476.
[20] R.B. Kellogg and M. Stynes, *Layers and corner singularities in singularly perturbed elliptic problems*, BIT 48 (2008), pp. 309–314.
[21] A.L. Mazzucato, V. Nistor and Q. Qu, *A nonconforming generalized finite element method for transmission problems*, SIAM J. Numer. Anal. 51 (2013), pp. 555–576.
[22] A.L. Mazzucato, V. Nistor and Q. Qu, *Quasi-optimal rates of convergence for the generalized finite element method in polygonal domains*, J. Comput. Appl. Math. 263 (2014), pp. 466–477.
[23] N. Moës, J. Dolbow and T. Belytschko, *A finite element method for crack growth without remeshing*, Int. J. Numer. Meth. Eng. 46 (1999), pp. 131–151.
[24] R.E. O'Malley, *Singular perturbation analysis for ordinary differential equations*, Commun. Math. Inst., Rijksuniversiteit Utrecht 5 (1977).
[25] H.-G. Roos, M. Stynes and L. Tobiska, *Numerical Methods for Singularly Perturbed Differential Equations*, Springer, Berlin, 1996.
[26] S.-D. Shih and R.B. Kellogg, *Asymptotic analysis of a singular perturbation problem*, SIAM J. Math. Anal. 18 (1987), pp. 1467–1511.
[27] M. Stynes, *Steady-state convection-diffusion problems*, Acta. Numer. 14 (2005), pp. 445–508.